Nanoporous Graphene | Hot Paper

DOI: 10.1002/anie.201402662

High-Quality Three-Dimensional Nanoporous Graphene**

*Yoshikazu Ito, Yoichi Tanabe, H.-J. Qiu, Katsuaki Sugawara, Satoshi Heguri, Ngoc Han Tu, Khuong Kim Huynh, Takeshi Fujita, Takashi Takahashi, Katsumi Tanigaki, and Mingwei Chen**

Abstract: *We report three-dimensional (3D) nanoporous graphene with preserved 2D electronic properties, tunable pore sizes, and high electron mobility for electronic applications. The complex 3D network comprised of interconnected graphene retains a 2D coherent electron system of massless Dirac fermions. The transport properties of the nanoporous graphene show a semiconducting behavior and strong pore-size dependence, together with unique angular independence. The free-standing, large-scale nanoporous graphene with 2D electronic properties and high electron mobility holds great promise for practical applications in 3D electronic devices.*

Graphene is a massless Dirac fermion system with high electron mobility, which holds great promise for replacing silicon in future electronics.[1] For practical applications in devices, it is essential to construct the 2D materials in 3D configurations with preservation of graphene electronic properties. Herein, we report three-dimensional (3D) nanoporous monolayer graphene with 2D electronic properties, tunable pore sizes, and high electron mobility for electronic applications. The complex 3D network comprised of interconnected graphene retains a 2D coherent electron system of massless Dirac fermions. The transport properties of the nanoporous graphene show a semiconductor behavior and strong pore-size dependence, together with unique angular independence. Free-standing, large-scale nanoporous graphene with 2D electronic properties holds great promise for practical applications in 3D devices.

To construct the two-dimensional graphene into 3D structures, several approaches, such as template,[2] gel,[3] layer stack,[4] and chemical vapor deposition (CVD),[5] with controllable pore sizes and feasible fabrication, have recently been developed. Although those 3D graphene materials show excellent electrochemical, catalytic, optoelectronic, and mechanical properties, the unique physical characteristics of graphene, such as massless Dirac fermions with high electron mobility, cannot be well preserved owing to poor interconnectivity and high defect density, which precludes their application in electronics and spintronics. Herein we reveal a novel nanoporous Ni-based CVD approach to fabricate high-quality 3D nanoporous graphene, which allows us to tailor the pore size of 3D graphene. Marvelously, the 3D nanoporous graphene can preserve the distinctive 2D coherent electronic properties in the 3D nanostructure. The open porous structure with a bicontinuous porosity, small pore size, large surface area, and high electron mobility holds great promise for physical and chemical applications of nanoporous graphene.

The fabrication process of 3D nanoporous graphene is elucidated in Scheme 1. A nanoporous Ni (np-Ni) substrate with a thickness of ca. 30 μm was prepared by electrochemically leaching Mn from a $Ni_{30}Mn_{70}$ precursor in a weak acid solution.[6] The as-prepared np-Ni, with an average nanopore/ligament size of ca. 10 nm, was annealed at 900 °C for 5–30 min in a CVD system under a mixed atmosphere of H_2, Ar, and benzene.[7] The usage of benzene as the carbon source benefits the growth of high quality graphene with a low formation energy.[7b] Graphene uniformly grew on the surface of nanosized Ni ligaments, which became coarser during graphene growth at high temperatures. The size of the Ni ligaments, and thus the pore size of the graphene, can be tailored from 100 nm to 2.0 μm by controlling the CVD time and temperatures (Supporting Information, Figure S1). Figure 1a depicts the graphene@np-Ni synthesized at 900 °C for 5 min. After graphene growth, the averaged nanopore size of the np-Ni was measured to be ca. 210 nm within a wide distribution range of 100–300 nm by a fast Fourier method.[6b] The nanoporous graphene was exfoliated by chemically removing the np-Ni substrate in a hydrogen chloride solution (Figure 1b). The interconnected nanoporous structure of the bulk np-Ni was fully inherited by the 3D graphene (Figure 1c). Chemical analysis verified that residual Ni in the nanoporous graphene is less than 0.08 atom% (Figure S2).

[*] Dr. Y. Ito, Dr. H.-J. Qiu,[+] Dr. K. Sugawara,[+] Dr. S. Heguri, Dr. K. K. Huynh, Dr. T. Fujita, Prof. T. Takahashi, Prof. K. Tanigaki, Prof. M. Chen
WPI Advanced Institute for Materials Research
Tohoku University, Sendai 980-8577 (Japan)
E-mail: mwchen@wpi-aimr.tohoku.ac.jp
Homepage: http://www.wpi-aimr.tohoku.ac.jp/chen_labo/
Dr. Y. Tanabe,[+] Dr. N. H. Tu, Prof. T. Takahashi, Prof. K. Tanigaki
Department of Physics, Graduate School of Science
Tohoku University, Sendai, 980-8578 (Japan)
Prof. M. Chen
State Key Laboratory of Metal Matrix Composites
School of Materials Science and Engineering
Shanghai Jiao Tong University, Shanghai 200030 (China)
and
CREST (Japan) Science and Technology Agency
Saitama 332-0012 (Japan)

[+] These authors contributed equally to this work.

[**] We would like to thank Professors Toshiaki Enoki and Yoji Koike for valuable discussions, and Dr. Atsushi Unemoto for CVD safety advice. This work was sponsored by JST-CREST "Phase Interface Science for Highly Efficient Energy Utilization"; the fusion research funds of "World Premier International (WPI) Research Center Initiative for Atoms, Molecules and Materials", MEXT (Japan), a Grant-in-Aid for Scientific Research on Innovative Areas "Science of Atomic Layers" (25107003), and KAKENHI (24740216, 24656028, 23224010). H.-J.Q. is supported by the Japan Society for the Promotion of Science (JSPS) postdoctoral fellowship program (P12054).

Supporting information for this article is available on the WWW under http://dx.doi.org/10.1002/anie.201402662.

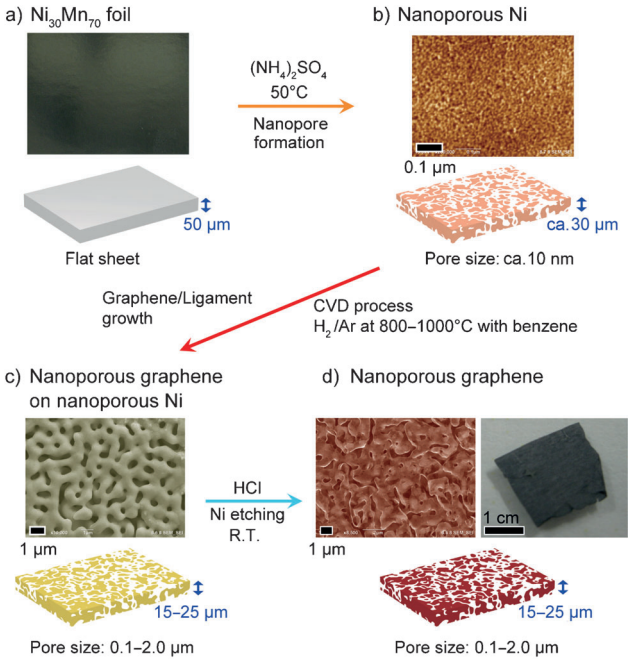

Scheme 1. a) Image of $Ni_{30}Mn_{70}$ foil. b) SEM image of nanoporous Ni after dealloying. c) SEM image of nanoporous graphene on nanoporous Ni after CVD at 900 °C for 5–30 min. d) SEM and optical images of nanoporous graphene after removing the nanoporous Ni substrate using a HCl solution.

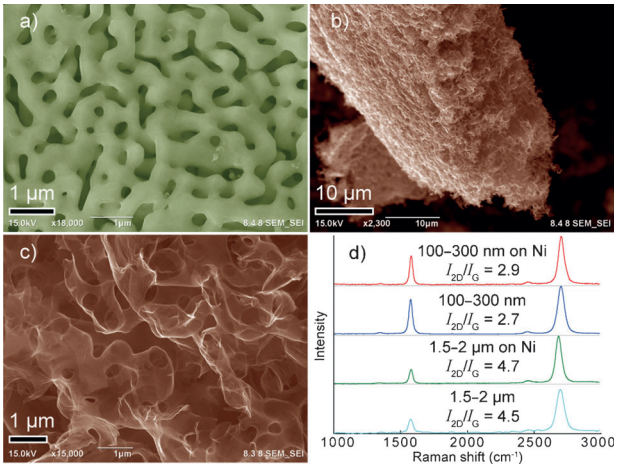

Figure 1. a) SEM images of nanoporous graphene on nanoporous Ni grown at 900 °C for 5 min. SEM images of nanoporous graphene, b) overview and c) close-up, after removing the nanoporous Ni substrate. d) Raman spectra of nanoporous graphene with and without Ni substrates. The 1.5–2.0 μm sample was prepared by CVD at 900 °C for 30 min.

The pore size of the nanoporous graphene was measured by using the Barrett-Joyner-Hallender (BJH) method.[8] As shown in Figure S3, the mean pore size of the graphene sample is ca. 200 nm, which is fairly consistent with that of the nanoporous Ni substrate. The quality of the nanoporous graphene was characterized by Raman spectroscopy. As shown in Figure 1 d, the sharp 2D bands, together with the high intensity ratio between the 2D and G bands, indicates that the 3D nanoporous sample is high-quality monolayered graphene.[1e,9] We have randomly probed the different regions of the nanoporous sample. The intensity ratio between the 2D and G bands remains nearly constant (Figure S4), demonstrating that the 3D nanoporous structure is mainly constructed by monolayered graphene. There is no obvious change in the graphene Raman bands after removing the np-Ni substrates, which suggests that chemical exfoliation does not introduce noticeable structural damage to the nanoporous graphene. It can be self-supported as a free-standing bulk material for device applications. The appearance of weak D bands in the Raman spectra (Figure 1 d) indicates the existence of structural defects in the 3D nanoporous graphene, which most likely originate from the curved parts of the graphene sheets, which are geometrically required to coordinate the 3D nanoporosity. Therefore, a smaller pore size with a larger curvature gradient gives rise to relatively stronger D band intensity, a lower I_{2D}/I_G ratio, and larger upward shift of the Raman 2D band.

The structure of nanoporous graphene was inspected by scanning transmission electron microscopy (STEM). The low-magnification bright-field STEM image (Figures 2 a and S5) shows the complex 3D morphology of the nanoporous graphene with concave and convex curvatures and nanopores, which is consistent with SEM observations. The selected area electron diffraction (inset in Figure 2 a) reveals that the 3D graphene has multiple orientations, which is associated with the random distribution of the interconnected graphene sheets in three dimensions. The atomic structure of the nanoporous graphene, as imaged by high-resolution TEM (HR-TEM) and BF-STEM, shows that the majority of the 3D graphene has a perfect hexagonal structure, the same as flat 2D graphene (Figure 2 b).[1b,10] However, pronounced topological defects, such as 5–7 defects,[10,11] can be observed in the regions where there is a large curvature gradient (marked by the yellow lines in Figure 2 c) between concave and convex sheets and the edges of nanopores. These atomic-scale defects are geometrically required to manage the 3D nanoporous configuration, and are evidently expected to affect the electronic structure and electric transport properties of the nanoporous graphene. Moreover, multilayer graphene (consisting of a few layers) can also be found, particularly at the neck parts of the interconnected nanopores.

The electronic structure of the nanoporous graphene with 100–300 nm and 1.5–2.0 μm pores was investigated by photoemission spectroscopy (PES). The valence band spectra of the two types of nanoporous graphene are shown in Figure 3 a. The overall features of the spectra are similar to that of 2D graphene, with a small band at ca. 3 eV and an intense band at 5–9 eV.[12] However, there are richer details in the spectra that 2D graphene does not have. Some of them are analogous to the prominent features of HOPG[13] (Figure 3 a), which may arise from some defective regions with bent lattices containing sp^3 configurations and local interlayer interactions in the 3D nanoporous structure. Importantly, there is a linear electronic density of states near the Fermi level (inset in Figure 3 a), which is consistent with the Dirac cone, thus indicating that the prevailing electronic properties of 3D nanoporous graphene preserve a 2D electron system of Dirac

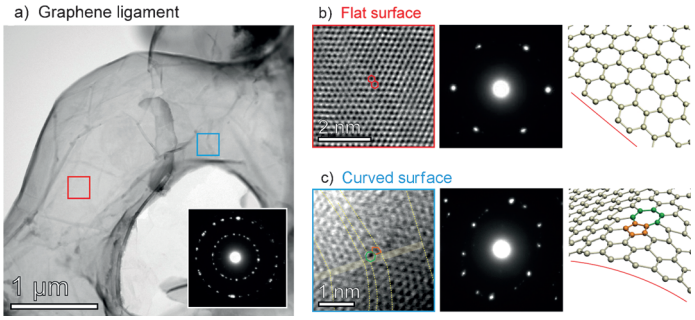

Figure 2. a) Typical low-magnification BF-STEM image of nanoporous graphene. The selected area electron diffraction pattern (inset) shows multiply orientated graphene sheets in the nanoporous configuration. b) HRTEM image and the electron diffraction pattern taken from the flat region of the nanoporous graphene. The atomic structure is consistent with the 2D model. c) The BF-STEM image and the electron diffraction patterns taken from a region with a large curvature gradient. The pentagon–heptagon pair lattices, together with large lattice bending, can be observed. The yellow dashed lines show the lattice directions.

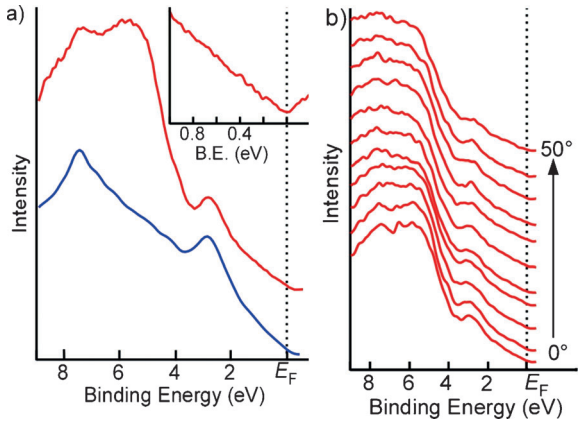

Figure 3. a) Angle-integrated photoemission spectra of 100–300 nm (blue) and 1.5–2.0 μm (red) porous graphene samples measured by a He IIα resonance line ($h\nu = 40.814$ eV) at room temperature. The inset shows the angle-integrated PES spectrum near the Fermi level divided by the Fermi–Dirac function convoluted with the instrumental energy resolution. b) Angle-resolved PES spectra of nanoporous graphene with pore sizes of 1.5–2.0 μm.

fermions particularly in the sample with a large pore size. Moreover, the pore-size dependence can be observed from the σ band at 5–9 eV. This may be due to the fact that small pores require more bent lattices with a sp^3 configuration to adopt the large curvature gradient.[14] Unlike 2D graphene, which has a strong angle dependence,[15] the angle-resolved PES spectra of the 3D nanoporous graphene does not show detectable changes with the emission angles (Figure 3b); this results from the randomly oriented graphene sheets in the complex nanoporous configuration. Therefore, the nanoporous graphene preserves 2D graphene electronic character in the 3D structure, and effectively eliminates the angular dependence that often limits applications in 3D devices.

The electric transport properties of the 3D nanoporous graphene with different pore sizes were experimentally evaluated and compared with those of 2D graphene. Figure 4 demonstrates the magnetic field (B) dependence of magnetoresistance as well as the temperature dependence of electronic conductance (σ), and mobility (μ). Although the quantum oscillation and magnetization ascribed to itinerant electrons may be suppressed owing to the asymmetric 3D network structure, as well as local defects in 3D nanoporous graphene (Figure S6), a linear magnetoresistance (LMR) is evidently confirmed in a wide temperature range for 3D nanoporous graphene with pore sizes of 1.5–2.0 μm. As LMR can be investigated as a characteristic of Dirac cones,[16] Dirac-cone-type linear electronic dispersion is considered to take place in the 3D interconnected graphene framework, which is consistent with the angle-integrated PES results discussed earlier (Figure 3a). At temperatures below 10 K, the 3D nanoporous graphene shows anomalous negative magnetoresistance at lower magnetic fields. This interesting transport phenomenon is not yet well understood, and may originate from local defects and domain

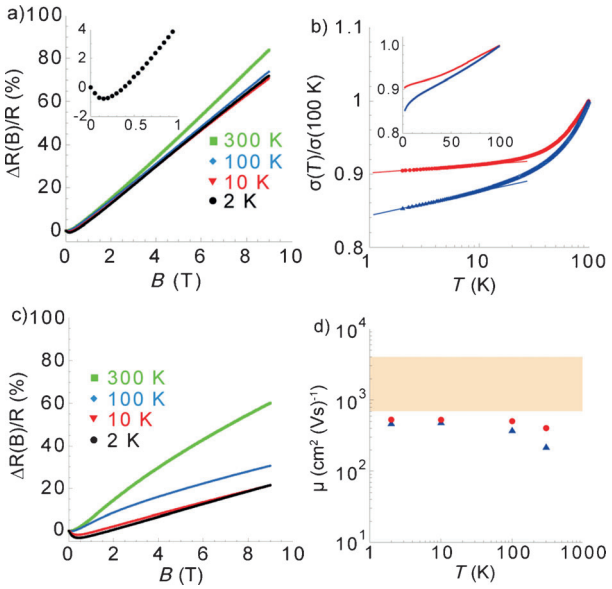

Figure 4. a) Magnetic field dependence of magnetoresistance (R(B)/R) of a 1.5–2.0 μm porous graphene sample. The inset shows the magnified plot of R(B)/R at 2 K. b) Temperature (T) dependence of normalized electrical conductance ($\sigma(T)/\sigma(100\ K)$) of 1.5–2.0 μm (red) and 100–300 nm (blue) nanoporous samples on a logarithmic scale. The experimental data were linearly fitted by the solid lines. The inset shows the T dependence of $\sigma(T)/\sigma(100\ K)$ in the linear scale. c) Magnetic field dependence of the magnetoresistance (R(B)/R) of a 100–300 nm nanoporous sample. d) Temperature dependence of the mobility (μ) of 1.5–2.0 μm (red) and 100–300 nm (blue) nanoporous graphene samples estimated from the single-carrier model. For comparison, the tan region represents the literature data on CVD 2D graphene.

structures in the 3D framework, which give rise to backscattering in 2D graphene sheets, or the effect from possible 3D Dirac fermions. In fact, a logarithmic decrease in the electrical conductance as a function of temperature was found at low temperatures, again demonstrating that the 2D electronic nature of graphene is preserved in the 3D nano-

porous framework (Figure 4b).[17] This observation distinguishes the 3D nanoporous graphene both from all other reported 3D carbon materials that do not have 2D electronic features,[18] and from sp^3-rich diamond films[19] For 100–300 nm porous graphene, a convex magnetoresistance (CMR) was observed at higher temperatures, which changes to LMR at lower temperatures, together with more obvious negative magnetoresistance at lower magnetic fields (Figure 4c). With smaller pore sizes the graphene sheet is more deformed and the contribution of the domain boundary and defects can be enhanced; this potentially opens the energy gap of the nanoporous graphene.[20] Consequently, it can be conceived that the CMR observed at high temperatures may be understood in the multicarrier transport of both the Dirac cone and the gapped parabolic band, and the carrier transport of the parabolic band is strongly suppressed owing to the potential scattering arising from the local defects and the domain structure, thus resulting in LMR at low temperatures. The electron mobility of the 3D nanoporous graphene was estimated under the assumption of a single carrier model and compared with CVD 2D graphene reported in the literature. The mobility of the 3D graphene depends on the pore sizes, with larger pores yielding higher mobility. The overall mobility of the 3D nanoporous graphene (Figure 4d) is lower than that of the CVD 2D graphene (700–4000 $cm^2(Vs)^{-1}$),[1e,21] mainly due to the topological defects and 3D geometry. However, the mobility is still sufficiently high for making 3D electronic devices, in particular, with configurations that cannot be created from the 2D graphene sheets.

In summary, we have successfully developed a nanoporous Ni-based CVD technique for the growth of high-quality 3D nanoporous graphene with tunable pore sizes from ca. 100 nm to ca. 2.0 μm, as well as coherent quantum electronic properties in the interconnected 3D structure. The nanoporous graphene preserves the massless Dirac fermion system, whereas the PES spectrum shows no significant angular dependence of photoelectron emission. The transport properties of 3D graphene demonstrate the Dirac cone electronic states without the quantum Hall effect, which reflects the uniqueness of the 3D interconnected graphene structure. The high electron mobility of the nanoporous graphene with preserved intrinsic 2D electronic characteristics at room temperature may pave a new way for the practical application of graphene in 3D devices in the future and for realizing high-dimensional Dirac fermion systems by 3D structure design of 2D graphene.

Received: February 24, 2014
Published online: March 28, 2014

Keywords: chemical vapor deposition · graphene · magnetoresistance · massless Dirac fermions · nanoporous materials

[1] a) K. S. Novoselov, A. K. Geim, S. V. Morozov, D. Jiang, M. I. Katsnelson, I. V. Grigorieva, S. V. Dubonos, A. A. Firsov, *Nature* **2005**, *438*, 197; b) A. H. C. Neto, F. Guinea, N. M. R. Peres, K. S. Novoselov, A. K. Geim, *Rev. Mod. Phys.* **2009**, *81*, 109; c) C. Berger, Z. Song, X. Li, X. Wu, N. Brown, C. Naud, D. Mayou, T. Li, J. Hass, A. N. Marchenkov, E. H. Conrad, P. N. First, W. Heer, *Science* **2006**, *312*, 1191; d) J. Wu, W. Pisula, K. Müllen, *Chem. Rev.* **2007**, *107*, 718; e) X. Li, W. Cai, J. An, S. Kim, J. Nah, D. Yang, R. Piner, A. Velamakanni, I. Jung, E. Tutuc, S. K. Banerjee, L. Colombo, R. S. Ruoff, *Science* **2009**, *324*, 1312; f) X. Huang, Z. Zeng, Z. Fan, J. Liu, H. Zhang, *Adv. Mater.* **2012**, *24*, 5979 – 6004; g) X. Huang, Z. Yin, S. Wu, X. Qi, Q. He, Q. Zhang, Q. Yan, F. Boey, H. Zhang, *Small* **2011**, *7*, 1876 – 1902; h) Q. He, S. Wu, Z. Yina, H. Zhang, *Chem. Sci.* **2012**, *3*, 1764 – 1772.

[2] a) W. Li, S. Gao, L. Wu, S. Qiu, Y. Guo, X. Geng, M. Chen, S. Liao, C. Zhu, Y. Gong, M. Long, J. Xu, X. Wei, M. Sun, L. Liu, *Sci. Rep.* **2013**, *3*, 2125; b) Z.-S. Wu, Y. Sun, Y.-Z. Tan, S. Yang, X. Feng, K. Müllen, *J. Am. Chem. Soc.* **2012**, *134*, 19532 – 19535; c) B. G. Choi, M. Yang, W. H. Hong, J. W. Choi, Y. S. Huh, *ACS Nano* **2012**, *6*, 4020 – 4028; d) Y. Li, Z. Li, P. K. Shen, *Adv. Mater.* **2013**, *25*, 2474 – 2480.

[3] a) Y. Xu, Z. Lin, X. Huang, Y. Liu, Y. Huang, X. Duan, *ACS Nano* **2013**, *7*, 4042 – 4049; b) W. Chen, S. Li, C. Chen, L. Yan, *Adv. Mater.* **2011**, *23*, 5679; c) W. Lv, Y. Tao, W. Ni, Z. Zhou, F.-Y. Su, X.-C. Chen, F.-M. Jina, Q.-H. Yang, *J. Mater. Chem.* **2011**, *21*, 12352 – 12357; d) Y. Xu, Z. Lin, X. Huang, Y. Wang, Y. Huang, X. Duan, *Adv. Mater.* **2013**, *25*, 5779 – 5784.

[4] X. Yang, C. Cheng, Y. Wang, L. Qiu, D. Li, *Science* **2013**, *341*, 534.

[5] a) Z. Chen, W. L. Gao, B. Liu, S. Pei, H.-M. Cheng, *Nat. Mater.* **2011**, *10*, 424; b) X. Cao, Y. Shi, W. Shi, G. Lu, X. Huang, Q. Yan, Q. Zhang, H. Zhang, *Small* **2011**, *7*, 3163 – 3168; c) X. Cao, Z. Zeng, W. Shi, P. Yep, Q. Yan, H. Zhang, *Small* **2013**, *9*, 1703 – 1707; d) X. Cao, Y. Shi, W. Shi, X. Rui, Q. Yan, J. Kong, H. Zhang, *Small* **2013**, *9*, 3433 – 3438; e) W. Zhou, X. Cao, Z. Zeng, W. Shi, Y. Zhu, Q. Yan, H. Liu, J. Wang, H. Zhang, *Energy Environ. Sci.* **2013**, *6*, 2216 – 2221; f) W. Li, S. Gao, L. Wu, S. Qiu, Y. Guo, X. Geng, M. Chen, S. Liao, C. Zhu, Y. Gong, M. Long, J. Xu, X. Wei, M. Sun, L. Liu, *Sci. Rep.* **2013**, *3*, 2125; g) S.-M. Yoon, W. M. Choi, H. Baik, H.-J. Shin, I. Song, M.-S. Kwon, J. J. Bae, H. Kim, Y. H. Lee, J.-Y. Choi, *ACS Nano* **2012**, *6*, 6803 – 6811; h) J.-S. Lee, H.-J. Ahn, J.-C. Yoon, J.-H. Jang, *Phys. Chem. Chem. Phys.* **2012**, *14*, 7938 – 7943; i) J.-S. Lee, S.-I. Kim, J.-C. Yoon, J.-H. Jang, *ACS Nano* **2013**, *7*, 6047 – 6055; j) D. A. C. Brownson, L. C. S. F-Filho, X. Ji, M. G-Mingot, J. Iniesta, O. Fatibello-Filho, D. K. Kampourisa, C. E. Banks, *J. Mater. Chem. A* **2013**, *1*, 5962 – 5972; k) L. Zhang, F. Zhang, X. Yang, G. Long, Y. Wu, T. Zhang, K. Leng, Y. Huang, Y. Ma, A. Yu, Y. Chen, *Sci. Rep.* **2013**, *3*, 1408; l) Y. He, W. Chen, X. Li, Z. Zhang, J. Fu, C. Zhao, E. Xie, *ACS Nano* **2013**, *7*, 174 – 182; m) Y. Zhang, M. Ma, J. Yang, W. Huang, X. Dong, *RSC Adv.* **2014**, *4*, 8466 – 8471.

[6] a) H.-J. Qiu, J. L. Kang, P. Liu, A. Hirata, T. Fujita, M. W. Chen, *J. Power Sources* **2014**, *247*, 896; b) T. Fujita, M. W. Chen, *Jpn. J. Appl. Phys.* **2008**, *47*, 1161.

[7] a) Y. Ito, C. Christodoulou, M. V. Nardi, N. Koch, H. Sachdev, K. Müllen, *ACS Nano* DOI: 10.1021/nn405661b; b) Z. Li, P. Wu, C. Wang, X. Fan, W. Zhang, X. Zhai, C. Zeng, Z. Li, J. Yang, J. Hou, *ACS Nano* **2011**, *5*, 3385.

[8] E. P. Barrett, L. G. Joyner, P. H. Halenda, *J. Am. Chem. Soc.* **1951**, *73*, 373.

[9] A. C. Ferrari, J. C. Meyer, V. Scardaci, C. Casiraghi, M. Lazzeri, F. Mauri, S. Piscanec, D. Jiang, K. S. Novoselov, S. Roth, A. K. Geim, *Phys. Rev. Lett.* **2006**, *97*, 187401.

[10] P. Y. Huang, C. S. Vargas, A. M. Zande, W. S. Whitney, M. P. Levendorf, J. W. Kevek, S. Garg, J. S. Alden, C. J. Hustedt, Y. Zhu, J. Park, P. L. McEuen, D. A. Muller, *Nature* **2011**, *469*, 389.

[11] C. G. Navarro, J. C. Meyer, R. S. Sundaram, A, Chuvilin, S. Kurasch, M. Burghard, K. Kern, U. Kaiser, *Nano Lett.* **2010**, *10*, 1144.

[12] K. R. Knox, S. Wang, S. Morgante, D. Cvetko, A. Locatelli, T. O. Mentes, M. A. Nino, P. Kim, R. M. Osgood, *Phys. Rev. B* **2008**, *78*, 201408.
[13] T. Haensel, A. Comouth, P. Lorenz, S. I. U. Ahmed, S. Krischok, N. Zydziak, A. Kauffmann, J. A. Schaefer, *Appl. Surf. Sci.* **2009**, *255*, 8183.
[14] T. Takahashi, H. Tokailin, T. Sagawa, *Phys. Rev. B* **1985**, *32*, 8317.
[15] a) A. Bostwick, T. Ohta, T. Seyller, K. Horn, E. Rotemberg, *Nat. Phys.* **2007**, *3*, 36; b) K. Sugawara, T. Sato, K. Kanetani, T. Takahashi, *J. Phys. Soc. Jpn.* **2011**, *80*, 024705.
[16] a) A. A. Abrikosov, *Phys. Rev. B* **1998**, *58*, 2788; b) A. L. Friedman, J. L. Tedesco, P. M. Campbell, J. C. Culbertson, E. Aifer, F. K. Perkins, R. M. Ward, J. K. Hite, C. R. Eddy, G. G. Jernigan, D. K. Gaskill, *Nano Lett.* **2010**, *10*, 3962.
[17] P. W. Anderson, E. Abrahams, T. V. Ramakrishnan, *Phys. Rev. Lett.* **1979**, *43*, 718.
[18] Y. Koike, S. Morita, T. Nakanomyo, T. Fukase, *J. Phys. Soc. Jpn.* **1985**, *54*, 713.
[19] W. L. Wang, K. J. Liao, B. B. Wang, *Diamond Relat. Mater.* **2000**, *9*, 1612 – 1616.
[20] a) G. Gui, J. Li, J. Zhong, *Phys. Rev. B* **2008**, *78*, 075435; b) F. Guinea, M. I. Katsnelson, M. A. H. Vozmediano, *Phys. Rev. B* **2008**, *77*, 075422.
[21] a) Y. Lee, S. Bae, H. Jang, S. Jang, S.-E. Zhu, S. H. Sim, H. Song, B. H. Hong, J.-H. Ahn, *Nano Lett.* **2010**, *10*, 490; b) M. P. Levendorf, C. S. Vargas, S. Garg, J. Park, *Nano Lett.* **2009**, *9*, 4479.

